Ozone-forced Southern Annular Mode during Antarctic Stratospheric Warming Events

Martin Jucker[1,1,1,1] and Rishav Goyal[1,1,1,1]

[1]University of New South Wales

November 30, 2022

Abstract

In 2019 southern hemisphere spring, a strong stratospheric warming event was predicted to force the southern annular mode (SAM) into a negative phase and adversely impact surface weather and Australian bushfire season for several months. Even though the negative SAM materialized towards late spring and summer, it was delayed by more than a month compared to model forecasts. Instead, the immediate surface response was a positive SAM through September and much of October. Here we show that the immediate surface response was a result of circulation changes forced by anomalously high ozone concentrations which occur during stratospheric warming events. The longer term tropospheric response was well predicted and is due to a different process acting on longer time scales. Capturing this coupling between dynamics and radiation in models is only possible with the inclusion of interactive ozone, which explains why most seasonal forecasting systems failed to capture it.

Ozone-forced Southern Annular Mode during Antarctic Stratospheric Warming Events

M. Jucker[1], **R. Goyal**[1]

[1]Climate Change Research Centre and ARC Centre of Excellence for Climate Extremes, University of New South Wales, Sydney, Australia

Key Points:

- Antarctic weak vortex events can force a positive tropospheric Southern Annular Mode via radiative forcing due to high ozone concentration.
- This heating increases lower stratospheric static stability, causing a wave-driven overturning circulation to develop in the troposphere.
- This mechanism is instantaneous and opposite the response usually associated with weak vortex dynamics.

Corresponding author: Martin Jucker, `publications@martinjucker.com`

Abstract

Southern Hemisphere (SH) Stratospheric Warming Events (SWEs) are usually associated with a negative phase of the tropospheric Southern Annular Mode (SAM) during the following summer. In contrast, using ensemble climate model simulations we show that the anomalously high ozone concentrations typically occurring during SWEs can force periods of persistent positive tropospheric SAM in austral spring by increasing lower stratospheric static stability and changing troposphere-to-stratosphere wave propagation. Eventually, the tropospheric SAM switches sign to its negative phase in late spring/early summer, but this 'downward propagation' of the stratospheric signal does not occur in simulations without seasonal cycle. We find that the downward propagation is forced both dynamically by adiabatic heating and radiatively by increased shortwave absorption by ozone due to the seasonal cycle. Capturing this ozone forcing mechanism in models requires the inclusion of interactive ozone, which has important implications for the predictive skill of current seasonal forecasting systems.

Plain Language Summary

In September of 2019, a rare event in the upper atmosphere was predicted to influence surface weather and worsen Australian bushfire season for several months. Even though that surface impact eventually appeared, it was delayed by more than a month compared to forecasts. Instead, the immediate surface response was opposite to what was expected through September to early October. Here we connect the immediate surface response to the unusually high ozone concentrations (anomalously small ozone hole) which generally occur during such stratospheric events. This points to a potential for better seasonal forecasts as current forecasting systems do not include the role of year-to-year variability in stratospheric ozone.

1 Introduction

The spring 2019 stratospheric warming event (SWE) in the Southern Hemisphere (SH) was accompanied by a vertical dipole in polar cap (60-90°S) geopotential height throughout September and early October, with positive anomalies in the stratosphere and negative anomalies in the troposphere (Fig. 1a). As the event evolved in time, the stratospheric positive anomalies started to descend, and by late October the tropospheric anomalies switched signs to become positive as well (1a). Positive polar cap geopotential height anomalies correspond to the negative phase of the Northern and Southern Annular Modes (NAM/SAM) (Gerber et al., 2010) and have long been associated with SWEs (Baldwin & Dunkerton, 2001). SWEs have attracted interest for their potential to improve seasonal forecasting in both hemispheres (Sigmond et al., 2013; Domeisen et al., 2020; Lim et al., 2019). Specifically, the negative phase of the SAM is associated with warmer and drier than usual conditions over much of Australia and South Africa, and the inverse for southern South America and New Zealand (Gillett et al., 2006).

However, the observation of a prominent and persistent positive phase of the tropospheric SAM in the spring of 2019 was surprising (Fig. 1), and in particular its persistence (∼5 weeks) made it extraordinary. Based on daily reanalysis data (ERA5, see Methods), the SAM was above 0.5 for periods longer than three weeks only six times in September-November (SON) since 1979, with one other occurrence during a year of an SWE (1988), and the last time more than 25 years ago in 1995. In contrast, most forecasting systems predicted a neutral SAM with a much faster transition to the negative phase during 2019 spring (Fig. 1c; Rao et al., 2020). Previous studies describe the specific conditions of 2019, including the evolution of the stratosphere (Safieddine et al., 2020; Lim, Hendon, Butler, et al., 2021), surface dynamics (Shen et al., 2020; Lim, Hendon, Shi, et al., 2021), and the performance of subseasonal to seasonal (S2S) forecasting systems (Rao et al., 2020). While most studies focus on the negative SAM in late spring

and summer of that year, Rao et al. (2020) found that the S2S systems generally failed to produce the positive SAM in spring, and Lim, Hendon, Shi, et al. (2021) suggested that the Indian Ocean Dipole (IOD) may have played some role in the delay of the negative SAM at the surface. As with any single event study, it is challenging to attribute a specific observation to (a) possible driver(s) of the observed tropospheric state in 2019 due to internal variability. Therefore, rather than conducting more analysis specific to that year, we will conduct numerical simulations in a more general setting and describe a novel mechanism whereby the strong increase in lower stratospheric ozone usually found during SWEs (Stolarski et al., 2005; Safieddine et al., 2020) forces a vertical dipole in the SAM with negative anomalies in the stratosphere and positive anomalies in the troposphere. We will use general circulation model ensemble simulations to remove effects of internal variability and crystallize the effects of enhanced stratospheric ozone on the phase of the SAM in austral spring.

A warmer and weaker stratospheric polar vortex during SWEs limits ozone-reducing chemical reactions, which together with the increased meridional transport of ozone rich air from the tropics are responsible for anomalously high stratospheric ozone concentrations (Randel & Cobb, 1994; Plumb, 2002; de la Cámara et al., 2018; Safieddine et al., 2020, and black line in Fig. 1b). While SWEs are often followed by a negative tropospheric SAM in December-February (DJF) (Thompson et al., 2005; Lim et al., 2019), the impact on the troposphere is not trivial. While most studies focus on surface impacts in DJF, or on longer-term trends related to ozone depletion and recovery, we will investigate the impact of ozone depletion during Austral spring compared to summer, on which there is far less research (Hurrel & Van Loon, 1994). Additionally, in contrast to the inter-annual or even inter-decadal timescales of ozone hole dynamics, we focus on dynamically induced ozone anomalies on the intra-seasonal timescale, usually related to SWEs. Our proposed mechanism relies on enhanced static stability just above the tropopause – forced by shortwave radiative heating due the anomalously high ozone concentrations – which then induces an anomalous circulation localized in the troposphere at midlatitudes corresponding to a positive tropospheric SAM.

2 Data and methods

2.1 Data and model

We use four different datasets for our analysis: Daily instantaneous pressure level data from ERA5 reanalysis (Hersbach et al., 2020), the sub-seasonal to seasonal (S2S) prediction dataset (Vitart et al., 2017) downloaded from the European Centre for Medium-Range Weather Forecasts (ECMWF), and two sets of simulations performed with the Community Atmosphere Model, Version 4 (CAM4; Neale et al., 2010), which is coupled to the Community Land Model Version 4 (CLM4; Oleson et al., 2010) and run with a 1.875×2.5 degree finite volume grid with 26 hybrid sigma levels up to 2.2 hPa. Although CAM4 is a low-top model, all processes of importance to this work are limited to the atmosphere well below the model top, and we do not expect that to have an impact on our conclusions. CAM4 is forced with fixed pre-industrial monthly climatological SSTs and sea-ice to make sure our results are not impacted by boundary conditions specific to 2019. In the first set of simulations, we run a full seasonal cycle, once with 2005-2015 three-dimensional monthly mean climatological ozone concentrations (CTRL), and once with 2019 three-dimensional monthly mean ozone concentrations (PERT). The 2005-2015 period has been chosen for the CTRL ozone to avoid strong trends due to ozone hole formation and recovery in the 1980s and 1990s, and 2019 ozone was used due to the strong and persistent stratospheric ozone perturbation. The choice of contemporary ozone rather than pre-industrial is to include reasonable ozone perturbations rather than synthetic forcing. We emphasize that the only difference between CTRL and PERT is the ozone forcing. Both simulations are run for 50 years and the last 30 years are used for the analysis presented in this study. The second model setup uses the same setup as the CTRL

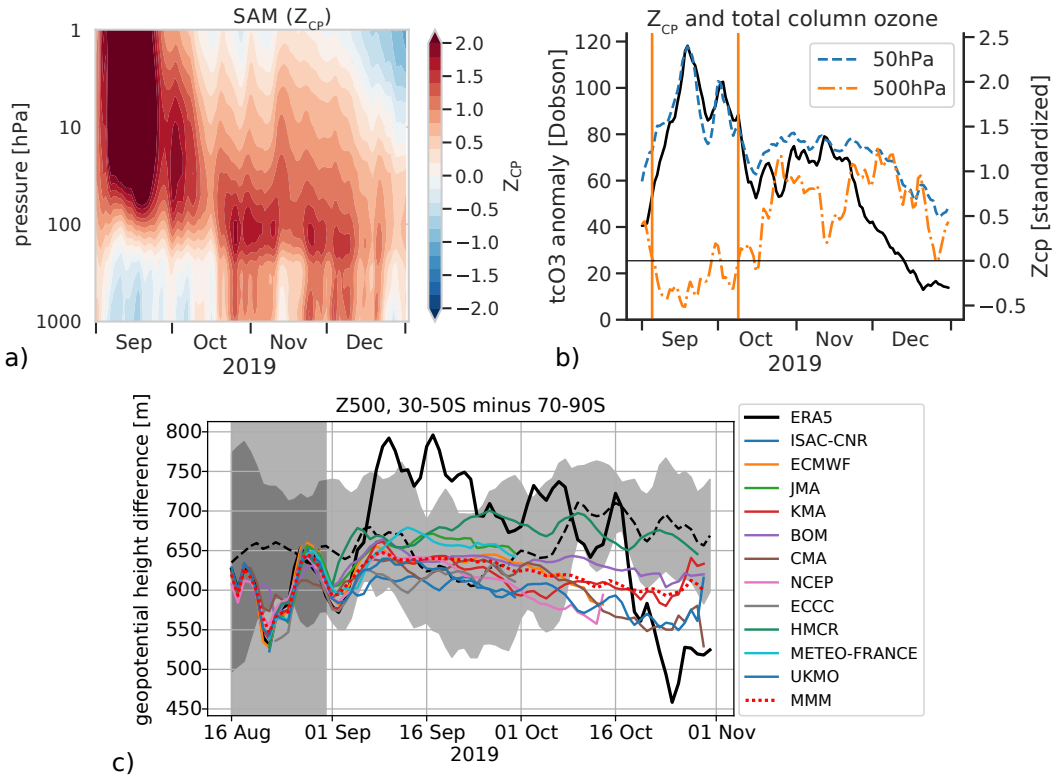

Figure 1. (a) Time-pressure plot of polar cap averaged standarized geopotential height anomalies Z_{CP} for Spring 2019 (red/blue meaning negative/positive SAM) in ERA5. (b) Same as (a), but for selected pressure levels at 50 hPa (blue/dashed) and 500 hPa (orange/dash-dotted). The black solid line in (b) shows the polar cap total column ozone anomaly relative to 2005-2015. The vertical lines show the time of interest when tropospheric SAM is positive. (c) S2S forecasts for all model initializations between 16 and 31 August (gray box). Shown is the 500 hPa geopotential height difference between 30-50S and 70-90S (positive meaning positive SAM) for 2019 in ERA5 (black line) and S2S models (colored continuous) as well as multi-model mean (red dashed). Model data was bias corrected for same mean as ERA5 during the second half of August (gray box). Black dashed line shows ERA5 2005-2015 climatology and gray shading one standard deviation during the same period.

simulation but we spin off 30 pairs of perpetual September simulations (fixed September mean ozone, SST, and equinox solar parameters) from September 1 of each year of the CTRL simulation. Again, the only difference between members for each initialization is 2005-2015 mean (CTRL-P) versus 2019 ozone (PERT-P). See Fig. S1 for an illustration of the ozone setup and difference in short wave forcing. The two different setups with and without seasonal cycle are designed to separate the effects of the seasonal cycle (where the polar vortex continuously weakens and eventually breaks down due to solar forcing) and the ozone forcing alone, but we will mainly focus on the simulations with seasonal cycle in this study. We entirely focus on the effect of increased stratospheric ozone, and do not try to estimate other possible mechanisms involved in the tropospheric response such as the role of cloud feedbacks (Grise et al., 2013; Maleska et al., 2020), influence of radiative effects on surface temperatures (Grise et al., 2009), or tropical modes of SST variability (recall that SSTs are fixed to pre-industrial control climatology). We remove effects of internal variability by averaging over our 30 ensemble members. Also note that by using monthly means for ozone, we miss the strong but short-lived peak in ozone concentration associated with the SWE (i.e. the ozone perturbation is weaker at ∼85 instead of up to ∼120 DU, see Fig. S1a), and the model only sees the full perturbation in mid-September, but we gain in signal-to-noise ratio thanks to a smoother ozone field and longer periods of anomalous heating.

2.2 Methods

The main diagnostic is the Southern Annular Mode (SAM), which we define as the standardized area-weighted polar cap (south of 60S) geopotential height anomaly at each pressure level. While the standardized first principle component of zonal mean geopotential height in the southern extratropics is often used (e.g. Thompson & Wallace, 1998; Baldwin & Dunkerton, 1999; Gerber et al., 2010), we follow Baldwin and Thompson (2009) who have shown that using the much simpler polar cap averaged geopotential height, henceforth denoted Z_{PC}, is well suited for stratosphere-troposphere coupling studies, and it allows direct comparison between our different datasets without having to compute principle components. To examine changes due to imposed increased stratospheric ozone concentrations in PERT, we define the climatology as the ensemble mean of CTRL for each day of the year and analyze the ensemble mean difference between the PERT and CTRL simulations during a particular interval of time. Statistical significance is assessed with a two-tailed t-test across all 30 PERT members against the null hypothesis of zero mean difference between PERT and CTRL and a significance level of 90%.

While the S2S dataset is not part of our dynamical analysis, it is still instructive to assess the predictions of state-of-the-art seasonal forecasting systems. We did not have access to model climatologies, nor is there a control simulation, which is why we compare the differences between 30-50S and 70-90S 500 hPa geopotential height on each day of the year in Fig. 1c. The details of how we define the SAM are of secondary importance for our analysis, as our proposed physical mechanism is ultimately based on various other dynamical variables.

We will use Eliassen-Palm fluxes (Eliassen & Palm, 1960; Andrews et al., 1983), downward control (Andrews et al., 1987; Haynes et al., 1991), the transformed Eulerian mean streamfunction (Andrews & McIntyre, 1978), and the static stability for our analysis. Eliassen-Palm fluxes are computed and scaled following (Jucker, 2021) and read

$$f_\phi = -\overline{u'v'}, \tag{1}$$

$$f_p = \left(f - \frac{1}{a\cos\phi}\frac{\partial(\bar{u}\cos\phi)}{\partial\phi}\right)\frac{\overline{v'\theta'}}{\bar{\theta}_p}, \tag{2}$$

and

$$\mathbf{F} \equiv (F_\phi, F_p) = a\cos\phi(f_\phi, f_p). \tag{3}$$

Here, u, v are the zonal and meridional wind, θ potential temperature, a Earth's radius and ϕ latitude. Overline ($\bar{\cdot}$) denotes zonal mean and prime ($'$) deviation from zonal mean. 'Downward control' refers to the findings from wave-mean flow interaction theory that the residual mean meridional overturning circulation is proportional to the vertical integral of wave activity flux above any given level (Andrews et al., 1987; Haynes et al., 1991):

$$\overline{\psi}^*(\phi, z) = \int_z^\infty \left. \frac{\rho_0 a \nabla \cdot \mathbf{F} \cos^2 \phi}{\overline{m}_\phi} \right|_{\phi=\phi(z')} \mathrm{d}z', \tag{4}$$

where ψ^* is the residual streamfunction in the latitude-height plane, ρ_0 is the density of air, z height and m_ϕ the angular momentum per unit mass. $\nabla \cdot \mathbf{F}$ is Eliassen-Palm flux divergence and represents the zonal force per unit mass exerted on the zonal flow by atmospheric waves (Andrews & McIntyre, 1976). The integral is taken along constant angular momentum $\overline{m_\phi}$, but in practice is done along constant latitude as contours of angular momentum are at nearly constant latitude (Haynes et al., 1991). Static stability is represented by the Brunt-Väisälä frequency $N^2 = g \mathrm{d} \ln \theta / \mathrm{d}z$, and we will refer to 'polar cap average' as the cosine-latitude weighted zonal and meridional mean south of 60S.

3 Results

As described above, we designed custom numerical experiments to test how stratospheric ozone anomalies may affect the tropospheric circulation, as lower stratospheric heating has been shown to have an influence on tropospheric dynamics (Simpson et al., 2009). A major difference between the model simulations and observations (besides interactive ozone) is that the models are not forced into producing an actual SWE, as radiative forcing from anomalous ozone is the only forcing in our experiments. While the polar vortex weakens in response to the heating, the latter is too weak to produce a 2019-like warming (Fig. S2). This approach allows us to distinguish the effects of the lower stratospheric heating associated with ozone from the dynamical heating involved in the lifecycle of an SWE, and our ensemble approach (using 30 ensemble members for each simulation) averages out the effects of internal variability. We note that to some extent the inverse experiment–i.e. dynamical heating without ozone anomalies–is represented by the S2S dataset, as those models produced an SWE but do not include interactive ozone, and failed to predict the positive SAM (Rao et al., 2020, and Fig. 1c).

The model setup which includes the seasonal cycle shows a vertical dipole of the correct sign in Z_{PC} anomalies starting from September (as seen during 2019, Fig. 1a), with a slowly downward propagating negative SAM (Fig. 2a). The downward propagation is what we will call the 'slow response' and corresponds to an early breakup of the polar vortex due to the additional ozone heating in PERT. We will discuss this below, and first concentrate on the 'fast' or immediate response (Fig. 2). We analyze the fast response by averaging over days 15 to 50, i.e. from mid-September to mid-October, as this is the initial period of statistically significant positive SAM anomalies in the troposphere (between vertical black lines in panel a). The model produces the positive SAM anomaly after September 15 because this is when it sees the full ozone anomalies in the PERT simulation due to linear interpolation of the monthly mean ozone concentrations used in the model. (Fig. S1).

In latitude-pressure space (Fig. 2b, shading), these springtime geopotential height anomalies correspond to the negative phase of the SAM in the stratosphere and the positive phase in the troposphere (Gerber & Vallis, 2009) . In the troposphere, there is a clockwise anomalous circulation (solid contours) centered around 50-70°S, which explains the negative geopotential height anomalies at high latitudes and positive anomalies in midlatitudes via upwelling at high latitudes and downwelling at lower latitudes. At the same time, there is anomalous equatorward Eliassen-Palm (EP) flux propagation in the upper troposphere and anomalous downward EP fluxes in the stratosphere around the

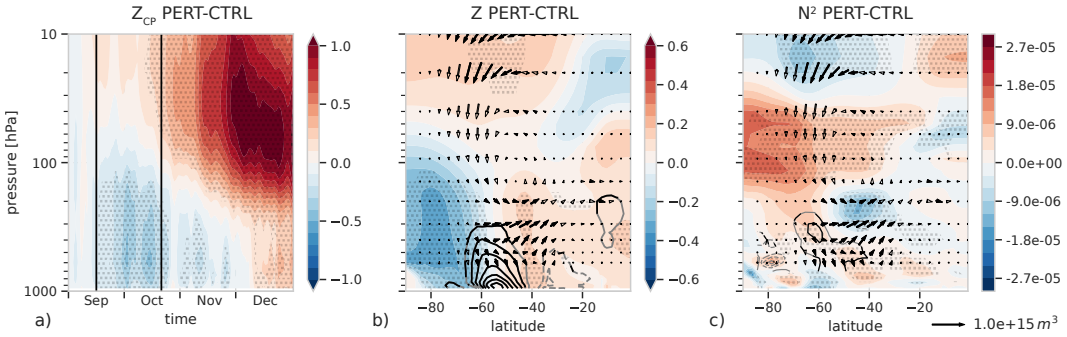

Figure 2. Composites of PERT anomalies. (a) Time-height evolution of Z_{PC}. (b) Geopotential height anomalies (shading), anomalous residual streamfunction (contours) and anomalous EP fluxes (arrows) for all days between September 15 and October 20 (vertical black lines in a). (c) Anomalies of static stability (shading), EP flux divergence (contours) and EP fluxes (arrows). Geopotential height is standardized, streamfunction is contoured in steps of 2e9 kg/s, EP flux divergence in multiples of $0.5\,\mathrm{ms}^{-1}\mathrm{d}^{-1}$. Significance is assessed using a two-tailed t-test and shading is stippled where significant at the 90% level. Streamfunction and divergence contours are black where significant and gray elsewhere, whereas EP flux arrows are filled where significant and hollow elsewhere. EP fluxes are computed and scaled following Jucker (2021), and they might appear as black dots where they are small. This is not to be confused with the gray stippling.

same latitudes (arrows), meaning that tropospheric EP fluxes are deviated equatorward instead of traveling into the stratosphere, creating positive EP flux divergence around the tropopause (panel 2c, solid contours). The EP flux divergence explains the clockwise circulation via downward control (Eq. 4) and thus the positive SAM. Finally, the reason why EP fluxes are deflected near the tropopause instead of propagating into the stratosphere is an increase in lower stratospheric stability, which extends from the pole northward to about 20°S and inhibits vertical wave propagation (Charney & Drazin, 1961). The increased static stability is due to anomalous ozone heating (panel 2c, shading).

This is similar to, but distinct from, a mechanism proposed earlier by Harnik and Lindzen (2001); Perlwitz and Harnik (2003, 2004) where time-lagged correlations were used to describe the reflection of waves in the upper stratosphere and a subsequent propagation back into the troposphere. These reflected waves then influence tropospheric wave structure on a time scale of about 12 days while wave-mean flow interactions influence the zonal mean tropospheric state on the long term. While the zonal wind geometry is susceptible to stratospheric wave reflection in our simulations in accordance with (Shaw et al., 2010), this is true for both CTRL and PERT, and the anomalies of PERT relative to CTRL do not show the time-lagged correlations described in that work (not shown). Furthermore, total EP fluxes (as opposed to anomalies) for both all waves and wave-1 are upward at all times (not shown), and Perlwitz and Harnik (2004) found that wave reflection did not influence the annular mode, which is the focus of our study. More importantly, Fig. 2 suggests that the important feature here is EP flux divergence near the tropopause, invoking downward control and therefore wave-mean flow rather than wave-wave interactions. Even so, it will be interesting to further study the relative roles of wave-wave and wave-mean flow interactions in this new context, even though separating the two might be more challenging given the important region is at the tropopause rather than high in the stratosphere, meaning any time lags due to vertical wave propagation would be very short.

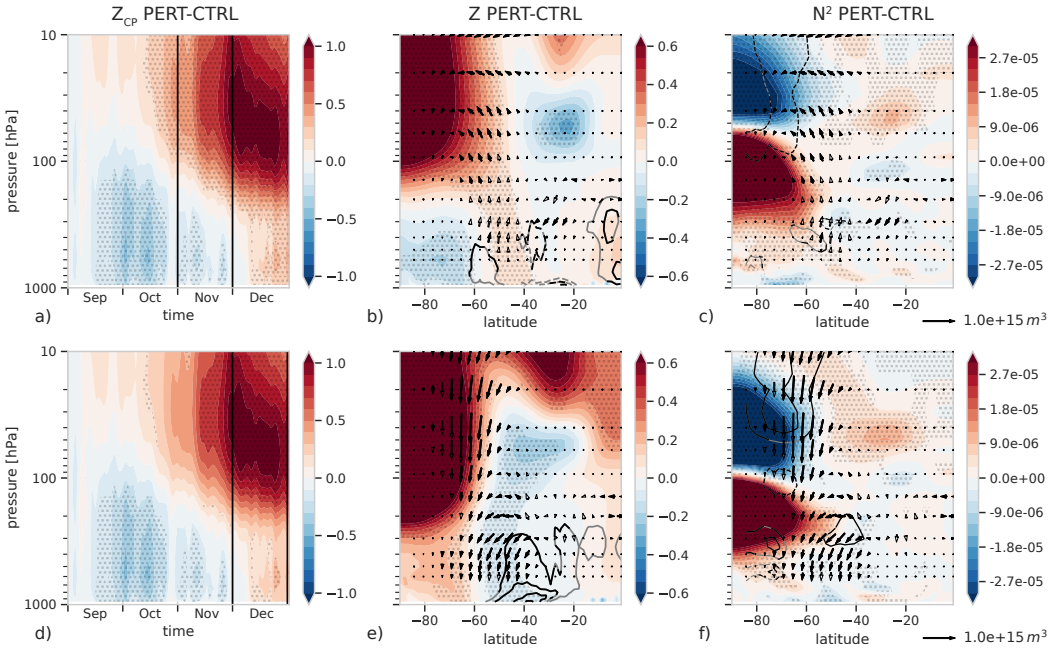

Figure 3. Same as Fig. 2 but for (top) November and (bottom) December.

At the same time as the fast response discussed above, a slower response develops which resembles the 'canonical' evolution of SWEs (Baldwin & Dunkerton, 2001; Charlton & Polvani, 2007; Jucker, 2016) (Fig. 3): After an initial fast dynamical response to stratospheric heating which takes place mostly in the troposphere, the polar vortex starts to weaken (Fig. 3 top) due to the short-wave heating associated with increased ozone and the seasonal cycle of solar radiation. During SWEs, the polar vortex would weaken more and faster due to adiabatic heating associated with an increased stratospheric overturning circulation. Either way, the result of this 'external' forcing (i.e. different from a simple increase in static stability due to ozone heating) is that the stability barrier in the lower stratosphere starts to erode and is now limited to regions south of 60°S, and the stratospheric polar vortex weakens above that, both leading to more upward EP flux in midlatitudes, a negative EP flux divergence in the stratosphere, and weakened EP flux divergence near the tropopause (panels 3b,c). Again invoking downward control, we can then understand the weakening of the clockwise tropospheric circulation and the positive SAM as a result of a partial cancelation between the clockwise drive from the upper tropospheric positive EP flux divergence and an anti-clockwise circulation driven by the negative EP flux divergence in the stratosphere (dashed lines in Fig. 3c).

After that (December, panels 3d-f), the polar vortex starts to break down, resulting in less upward EP flux throughout the atmosphere, and downward propagation of the negative SAM signature into the troposphere. In our model setup with seasonal cycle discussed here, this behavior corresponds to an early breakdown of the seasonal cycle rather than a sudden warming (Fig. S2). We note that by December, the differences in ozone concentration between PERT and CTRL become weak (Fig. S1), and the dynamics is now dictated by the early breakdown of the polar vortex. In the case of an SWE, the dynamically forced weakening of the polar vortex happens faster and we would expect the downward propagation due to the slow response to proceed earlier, with a surface impact in November or even October (depending on when the SWE occurs) instead of December. Even so, it is interesting that by the time the negative phase of the SAM reaches the troposphere (Fig. 3, bottom), the region of positive EP flux divergence in

the upper troposphere has moved further poleward and forces an anomalous clockwise circulation around 40°S, and given its more equatorward position compared to before, this now corresponds to a negative SAM (Figs. 3e,f). The anomalous wave drive (EP flux divergence) is still located near the (equatorward) edge of a region of increased static stability which has now reached the troposphere, and it will be subject to future work whether this is a general feature of 'downward propagating' stratospheric anomalies during early polar vortex breakdowns.

4 Summary and Discussion

The emerging picture of the mechanisms can be summarized as shown in Fig. 4. As a SWE is triggered, stratospheric ozone is transported from low to high latitudes. At the same time, the stratospheric polar vortex is both warmer and less isolated, inhibiting the formation of the ozone hole (Safieddine et al., 2020). Ozone concentrations increase most in the lower stratosphere and–if the event happens in the spring when enough sunlight is available–result in localized anomalous heating close to the tropopause. The heating of the lower stratosphere in turn increases the troposphere-stratosphere contrast in static stability, causing perturbations from the troposphere to deflect equatorward close to the tropopause rather than continuing vertically into the stratosphere (Chen & Robinson, 1992; Weinberger et al., 2021). Crucially, the deflection of EP fluxes creates anomalous divergence, which in turn forces a localized clockwise tropospheric circulation via downward control. That circulation includes anomalous upwelling over the polar cap and downwelling at lower latitudes, which projects onto the positive phase of the Southern Annular Mode.

Under the influence of the seasonal increase of insolation over high latitudes, the polar vortex weakens and descends more quickly through November when ozone concentrations are enhanced (PERT) compared to CTRL. At the same time, static stability anomalies are now more limited to high latitudes (poleward of 60°S), removing the mid-latitude propagation barrier for EP fluxes. As a result of both effects, more EP fluxes can propagate into the upper stratosphere and cause locally increased convergence (Fig. 3). More EP flux being able to propagate into the stratosphere means there is a decrease in anomalous EP flux divergence near the tropopause, and in addition we observe a mutual cancellation between the clockwise circulation driven by tropospheric EP flux divergence and the anti-clockwise circulation driven by stratospheric EP flux convergence (both via downward control). This marks the end of the fast response, and the subsequent evolution is dominated by the slow response.

We emphasize that while the fast response is forced by shortwave absorption via increased stratospheric ozone concentrations, the slow response requires a weakening of the stratospheric polar vortex via an additional forcing, which can either be dynamical heating associated with an SWE, or the seasonal increase in insolation. Indeed, there is no indication of a slow response and associated downward propagation in our perpetual September simulations, even though the mechanism inducing a positive SAM in the troposphere corresponding to the fast response is present throughout the simulation (Fig. S3).

During the slow response, the polar vortex continues its late spring descent, and stratospheric EP flux convergence becomes more important than tropospheric divergence, the negative SAM propagates downward similar to SWEs (Plumb & Semeniuk, 2003), and eventually forces an anomalous anti-clockwise circulation in the troposphere, resulting in a negative tropospheric SAM in summer. If there is a stronger (and possibly faster) external forcing, such as the dynamical heating from an SWE, the slow response can be expected to overpower the fast response earlier than in our simulations, and the tropospheric SAM would then switch sign to a negative phase in November or even October, rather than in December. It is worth recalling here that our simulations do not include interactive ozone, but impose ozone anomalies to assess their dynamical effects. The in-

terplay between dynamics and ozone could influence the balance between the fast and slow responses, but further work is required to explore this.

While we studied this mechanism in relation to strong ozone anomalies associated with weak vortex events, it does not have to be limited to such events and can be expected to be relevant whenever lower stratospheric static stability increases. For instance, Maleska et al. (2020) recently discussed a similar mechanism in the Northern Hemisphere (NH) and in the context of ozone depletion, whereby upper tropospheric static stability changes related to strong decreases in ozone impact high cloud amounts and surface temperatures via longwave cloud radiative effects. Thus, one direction for future work will be to analyze other occurrences of strong inversions above the tropopause. Given the role of shortwave heating in our mechanism, we might not expect a similar effect with mid-winter SWEs in the NH, but it could have an influence on NH late-winter SWEs. Recent work has highlighted differences in the surface impact of NH sudden stratospheric warmings when including interactive ozone (Haase & Matthes, 2019; Oehrlein et al., 2020), although these studies mainly discuss longer persistence of stratospheric anomalies with interactive ozone, and it is not clear from these studies whether stratospheric static stability plays an important role in the NH. Similarly, Thompson et al. (2006) found based on observational data that during SWEs in the NH, the effect of radiation alone is of opposite sign in the stratosphere and the troposphere and contributes to the persistence of the tropospheric response, although they only consider longwave cooling of the stratosphere as a response to dynamical heating of SWEs rather than the shortwave heating due to ozone discussed in our study. While they acknowledge a lack of understanding concerning the governing mechanism in their discussion, they also report on the importance of anomalous meridional tropospheric wave activity. More recently, White et al. (2020) reported short periods of positive NAM similar to our fast response when artificially forcing mid-winter sudden warmings with an idealized stratospheric heating profile in the NH, not unlike our fast response, although they do not conduct any further analysis to examine the mechanisms involved in producing such a dipole. While they do not include the effects of ozone explicitly, their artificially imposed heating profile might involuntarily mimic the effect of ozone similar to our fast response. Furthermore, as discussed in this paper, the S2S forecasting systems failed to produce the positive SAM in 2019 even though most models predicted the strong weakening of the polar vortex. We conclude that the exact form of the heating (meridional and vertical position) might matter, and this presents another direction for future work.

Coming back to the special case of spring 2019 which motivated this work, many of the dynamical features discussed here are clearly visible during the time of positive SAM in September and early October, in particular the enhanced lower stratospheric stability and associated anomalous EP flux divergence and the resulting clockwise tropospheric circulation (Fig. S4). While there certainly was an interplay with many other tropospheric phenomena during this particular event (Shen et al., 2020; Lim, Hendon, Shi, et al., 2021), we find it remarkable how similar the dynamics appear between our model simulations where stratospheric ozone is the only forcing and the observed atmospheric evolution. To conclude, our results indicate that including interactive ozone in forecasting systems should be expected to improve model performance not only during austral summer as previously reported (Rae et al., 2019; Hendon et al., 2020), but also during austral spring.

Acknowledgements

Both authors acknowledge support by the ARC Centre of Excellence for Climate Extremes which is supported by the Australian Research Council via grant CE170100023. MJ further acknowledges ARC grant FL150100035. This research was undertaken with the assistance of resources from the National Computational Infrastructure (NCI Australia), an NCRIS enabled capability supported by the Australian Government. We thank

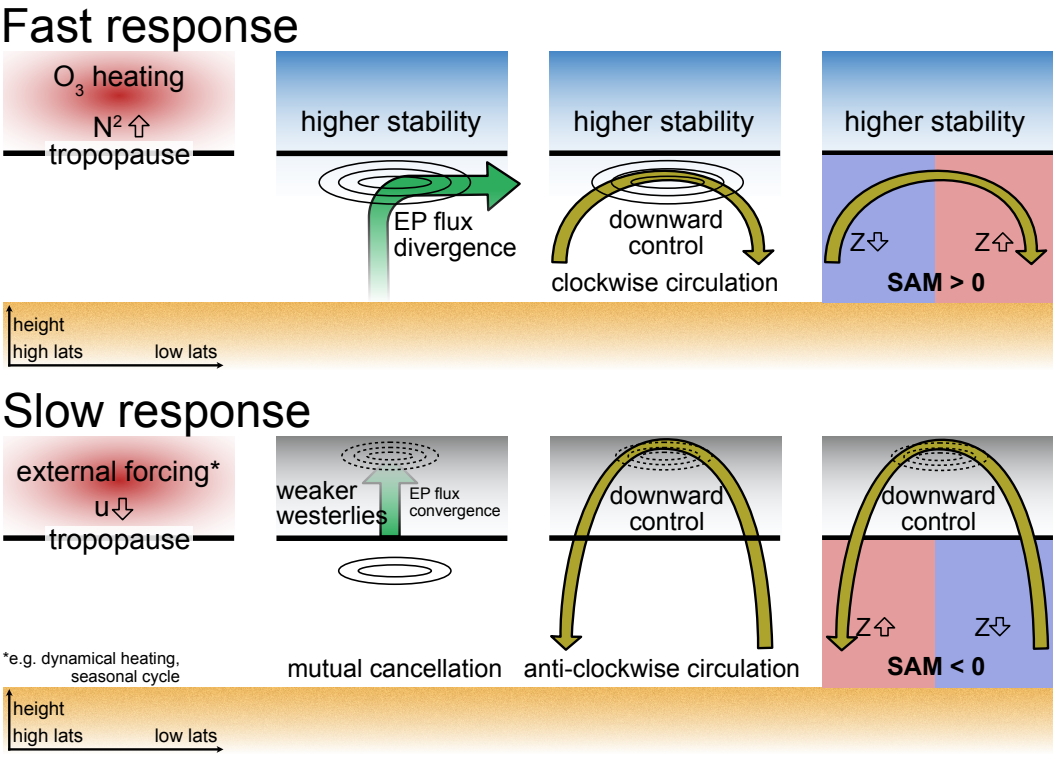

Figure 4. Schematic of the physical mechanism explaining the slow and fast responses to increased stratospheric ozone. The thick black line represents the tropopause in all panels. The fast response (top) forces a positive SAM in the troposphere, whereas the slow response (bottom) corresponds to a 'downward propagation' of the stratospheric signal which then induces a negative SAM in the troposphere, typically in early summer. See text for more details.

Amy Butler and Andrew Charlton-Perez for sharing the results from a SPARC survey of the implementation of ozone in S2S models.

Open Research

Model data and the necessary python scripts for creating all figures is available at `https://doi.org/10.5281/zenodo.5120971` (Jucker & Goyal, 2021). The data repository also includes descriptions for each entry and instructions for reproduction of the results presented here.

References

Andrews, D. G., Holton, J. R., & Leovy, C. B. (1987). *Middle Atmosphere Dynamics*. San Diego: Academic Press.

Andrews, D. G., Mahlman, J. D., & Sinclair, R. W. (1983, 12). Eliassen-Palm Diagnostics of Wave-Mean Flow Interaction in the GFDL "SKYHI" General Circulation Model. *Journal of the Atmospheric Sciences*, *40*(12), 2768–2784. doi: 10.1175/1520-0469(1983)040⟨2768:ETWATM⟩2.0.CO;2

Andrews, D. G., & McIntyre, M. E. (1976, 11). Planetary Waves in Horizontal and Vertical Shear: The Generalized Eliassen-Palm Relation and the Mean Zonal Acceleration. *Journal of the Atmospheric Sciences*, *33*(11), 2031–2048. doi: 10.1175/1520-0469(1976)033⟨2031:PWIHAV⟩2.0.CO;2

Andrews, D. G., & McIntyre, M. E. (1978). Generalized Eliassen-Palm and Charney-Drazin Theorems for Waves oin Axismmetric Mean Flows in Compressible Atmospheres. *Journal of Atmospheric Sciences*, *35*, 175. doi: 10.1175/1520-0469(1978)035⟨0175:gepacd⟩2.0.co;2

Baldwin, M. P., & Dunkerton, T. J. (1999, 12). Propagation of the Arctic Oscillation from the stratosphere to the troposphere. *Journal of Geophysical Research Atmospheres*, *104*(D24), 30937–30946. doi: 10.1029/1999JD900445

Baldwin, M. P., & Dunkerton, T. J. (2001, 10). Stratospheric harbingers of anomalous weather regimes. *Science (New York, N.Y.)*, *294*(5542), 581–4. doi: 10.1126/science.1063315

Baldwin, M. P., & Thompson, D. W. (2009, 10). A critical comparison of stratosphere-troposphere coupling indices. *Quarterly Journal of the Royal Meteorological Society*, *135*(644), 1661–1672. doi: 10.1002/qj.479

Charlton, A. J., & Polvani, L. M. (2007, 2). A New Look at Stratospheric Sudden Warmings. Part I: Climatology and Modeling Benchmarks. *Journal of Climate*, *20*(3), 449–469. doi: 10.1175/JCLI3996.1

Charney, J., & Drazin, P. (1961). Propagation of Planetary-Scale Disturbances from the Lower into the Upper Atmosphere. *J. Geophys. Res*, *66*, 83–109.

Chen, P., & Robinson, W. A. (1992, 12). Propagation of planetary waves between the troposphere and stratosphere. *Journal of Atmospheric Sciences*, *49*(24), 2533. doi: 10.1175/1520-0469(1992)049⟨2533:POPWBT⟩2.0.CO;2

de la Cámara, A., Abalos, M., Hitchcock, P., Calvo, N., & Garcia, R. R. (2018, 11). Response of Arctic ozone to sudden stratospheric warmings. *Atmospheric Chemistry and Physics*, *18*(22), 16499–16513. doi: 10.5194/acp-18-16499-2018

Domeisen, D. I., Butler, A. H., Charlton-Perez, A. J., Ayarzagüena, B., Baldwin, M. P., Dunn-Sigouin, E., ... Taguchi, M. (2020). The Role of the Stratosphere in Subseasonal to Seasonal Prediction: 2. Predictability Arising From Stratosphere-Troposphere Coupling. *Journal of Geophysical Research: Atmospheres*, *125*(2), 1–20. doi: 10.1029/2019JD030923

Eliassen, A., & Palm, T. (1960). On the transfer of energy in stationary mountain waves. *Geofys. Publ.*, *22*(3), 1–23.

Gerber, E. P., Baldwin, M. P., Akiyoshi, H., Austin, J., Bekki, S., Braesicke, P., ... Smale, D. (2010). Stratosphere-troposphere coupling and annular mode variability in chemistry-climate models. *Journal of Geophysical Research Atmospheres*, *115*(18), 1–15. doi: 10.1029/2009JD013770

Gerber, E. P., & Vallis, G. K. (2009, 2). On the Zonal Structure of the North Atlantic Oscillation and Annular Modes. *Journal of the Atmospheric Sciences*, *66*(2), 332–352. doi: 10.1175/2008JAS2682.1

Gillett, N. P., Kell, T. D., & Jones, P. D. (2006). Regional climate impacts of the Southern Annular Mode. *Geophysical Research Letters*, *33*(23), 1–4. doi: 10.1029/2006GL027721

Grise, K. M., Polvani, L. M., Tselioudis, G., Wu, Y., & Zelinka, M. D. (2013, 7). The ozone hole indirect effect: Cloud-radiative anomalies accompanying the

poleward shift of the eddy-driven jet in the Southern Hemisphere. *Geophysical Research Letters*, *40*(14), 3688–3692. doi: 10.1002/grl.50675

Grise, K. M., Thompson, D. W. J., & Forster, P. M. (2009, 8). On the Role of Radiative Processes in Stratosphere–Troposphere Coupling. *Journal of Climate*, *22*(15), 4154–4161. doi: 10.1175/2009JCLI2756.1

Haase, S., & Matthes, K. (2019). The importance of interactive chemistry for stratosphere-troposphere coupling. *Atmospheric Chemistry and Physics*, *19*(5), 3417–3432. doi: 10.5194/acp-19-3417-2019

Harnik, N., & Lindzen, R. S. (2001, 10). The Effect of Reflecting Surfaces on the Vertical Structure and Variability of Stratospheric Planetary Waves. *Journal of the Atmospheric Sciences*, *58*(19), 2872–2894. doi: 10.1175/1520-0469(2001)058⟨2872:TEORSO⟩2.0.CO;2

Haynes, P. H., McIntyre, M. E., Shepherd, T. G., Marks, C. J., & Shine, K. P. (1991, 2). On the "Downward Control" of Extratropical Diabatic Circulations by Eddy-Induced Mean Zonal Forces. *Journal of the Atmospheric Sciences*, *48*(4), 651–678. doi: 10.1175/1520-0469(1991)048⟨0651:OTCOED⟩2.0.CO;2

Hendon, H. H., Lim, E. P., & Abhik, S. (2020). Impact of Interannual Ozone Variations on the Downward Coupling of the 2002 Southern Hemisphere Stratospheric Warming. *Journal of Geophysical Research: Atmospheres*, *125*(16), 1–16. doi: 10.1029/2020JD032952

Hersbach, H., Bell, B., Berrisford, P., Hirahara, S., Horányi, A., Muñoz-Sabater, J., ... Thépaut, J. (2020, 7). The ERA5 global reanalysis. *Quarterly Journal of the Royal Meteorological Society*, *146*(730), 1999–2049. doi: 10.1002/qj.3803

Hurrel, J. W., & Van Loon, H. (1994, 5). A modulation of the atmospheric annual cycle in the Southern Hemisphere. *Tellus A*, *46*(3), 325–338. doi: 10.1034/j.1600-0870.1994.t01-1-00007.x

Jucker, M. (2016, 12). Are Sudden Stratospheric Warmings Generic? Insights from an Idealized GCM. *Journal of the Atmospheric Sciences*, *73*(12), 5061–5080. doi: 10.1175/JAS-D-15-0353.1

Jucker, M. (2021, 4). Scaling of Eliassen-Palm flux vectors. *Atmospheric Science Letters*, *22*(4), e1020. doi: 10.1002/asl.1020

Jucker, M., Goyal, R. (2021). Data for Jucker and Goyal, Ozone-forced Southern Annular Mode during Antarctic Stratospheric Warming Events, Geophysical Research Letters, submitted. *Zenodo*. doi: 10.5281/zenodo.5120971

Lim, E.-P., Hendon, H. H., Boschat, G., Hudson, D., Thompson, D. W. J., Dowdy, A. J., & Arblaster, J. M. (2019, 11). Australian hot and dry extremes induced by weakenings of the stratospheric polar vortex. *Nature Geoscience*, *12*(11), 896–901. doi: 10.1038/s41561-019-0456-x

Lim, E.-P., Hendon, H. H., Butler, A. H., Thompson, D. W. J., Lawrence, Z., Scaife, A. A., ... Wang, G. (2021, 2). The 2019 Southern Hemisphere stratospheric polar vortex weakening and its impacts. *Bulletin of the American Meteorological Society*, 1–50. doi: 10.1175/BAMS-D-20-0112.1

Lim, E. P., Hendon, H. H., Shi, L., de Burgh-Day, C., Hudson, D., King, A., ... Marshall, A. (2021). Tropical forcing of Australian extreme low minimum temperatures in September 2019. *Climate Dynamics*, *56*(11-12), 3625–3641. doi: 10.1007/s00382-021-05661-8

Maleska, S., Smith, K. L., & Virgin, J. (2020). Impacts of stratospheric ozone extremes on arctic high cloud. *Journal of Climate*, *33*(20), 8869–8884. doi: 10.1175/JCLI-D-19-0867.1

Neale, R. B., Richter, J. H., Conley, A. J., Park, S., Lauritzen, P. H., Gettelman, A., & Williamson, D. L. (2010). Description of the NCAR Community Atmosphere Model (CAM 4.0). *NCAR Technical Note*, *TN-485*(April), 1–196.

Oehrlein, J., Chiodo, G., & Polvani, L. M. (2020). The effect of interactive ozone chemistry on weak and strong stratospheric polar vortex events. *Atmospheric Chemistry and Physics*, *20*(17), 10531–10544. doi: 10.5194/

acp-20-10531-2020

Oleson, K. W., Lawrence, D. M., Bonan, G. B., Flanner, M. G., Kluzek, E., Lawrence, P. J., ... Thornton, P. E. (2010). Technical Description of version 4.0 of the Community Land Model (CLM). *NCAR Technical Note*, *TN-478*(April), 1–238. doi: http://dx.doi.org/10.5065/D6FB50WZ

Perlwitz, J., & Harnik, N. (2003). Observational evidence of a stratospheric influence on the troposphere by planetary wave reflection. *Journal of Climate*, *16*(18), 3011–3026. doi: 10.1175/1520-0442(2003)016⟨3011:OEOASI⟩2.0.CO;2

Perlwitz, J., & Harnik, N. (2004). Downward coupling between the stratosphere and troposphere: The relative roles of wave and zonal mean processes. *Journal of Climate*, *17*(24), 4902–4909. doi: 10.1175/JCLI-3247.1

Plumb, R. A. (2002). Stratospheric Transport. *J. Meteor. Soc. Japan*, *80*(1949), 793–809.

Plumb, R. A., & Semeniuk, K. (2003). Downward migration of extratropical zonal wind anomalies. *Journal of Geophysical Research*, *108*(D7), 4223. doi: 10.1029/2002JD002773

Rae, C. D., Keeble, J., Hitchcock, P., & Pyle, J. A. (2019). Prescribing Zonally Asymmetric Ozone Climatologies in Climate Models: Performance Compared to a Chemistry-Climate Model. *Journal of Advances in Modeling Earth Systems*, *11*(4), 918–933. doi: 10.1029/2018MS001478

Randel, W. J., & Cobb, J. B. (1994). Coherent variations of monthly mean total ozone and lower stratospheric temperature. *Journal of Geophysical Research*, *99*(D3), 5433. doi: 10.1029/93JD03454

Rao, J., Garfinkel, C. I., White, I. P., & Schwartz, C. (2020, 7). The Southern Hemisphere Minor Sudden Stratospheric Warming in September 2019 and its Predictions in S2S Models. *Journal of Geophysical Research: Atmospheres*, *125*(14). doi: 10.1029/2020JD032723

Safieddine, S., Bouillon, M., Paracho, A. C., Jumelet, J., Tencé, F., Pazmino, A., ... Clerbaux, C. (2020). Antarctic Ozone Enhancement During the 2019 Sudden Stratospheric Warming Event. *Geophysical Research Letters*, *47*(14), 1–10. doi: 10.1029/2020GL087810

Shaw, T. A., Perlwitz, J., & Harnik, N. (2010, 12). Downward Wave Coupling between the Stratosphere and Troposphere: The Importance of Meridional Wave Guiding and Comparison with Zonal-Mean Coupling. *Journal of Climate*, *23*(23), 6365–6381. doi: 10.1175/2010JCLI3804.1

Shen, X., Wang, L., & Osprey, S. (2020). Tropospheric Forcing of the 2019 Antarctic Sudden Stratospheric Warming. *Geophysical Research Letters*, *47*(20), 1–8. doi: 10.1029/2020GL089343

Sigmond, M., Scinocca, J. F., Kharin, V. V., & Shepherd, T. G. (2013, 1). Enhanced seasonal forecast skill following stratospheric sudden warmings. *Nature Geoscience*, *6*(2), 98–102. doi: 10.1038/ngeo1698

Simpson, I. R., Blackburn, M., & Haigh, J. D. (2009, 5). The Role of Eddies in Driving the Tropospheric Response to Stratospheric Heating Perturbations. *Journal of the Atmospheric Sciences*, *66*(5), 1347–1365. doi: 10.1175/2008JAS2758.1

Stolarski, R. S., McPeters, R. D., & Newman, P. A. (2005, 3). The Ozone Hole of 2002 as Measured by TOMS. *Journal of the Atmospheric Sciences*, *62*(3), 716–720. doi: 10.1175/JAS-3338.1

Thompson, D. J. W., Baldwin, M. P., & Solomon, S. (2005, 3). Stratosphere–Troposphere Coupling in the Southern Hemisphere. *Journal of the Atmospheric Sciences*, *62*(3), 708–715. doi: 10.1175/JAS-3321.1

Thompson, D. W., Furtado, J. C., & Shepherd, T. G. (2006). On the tropospheric response to anomalous stratospheric wave drag and radiative heating. *Journal of the Atmospheric Sciences*, *63*(10), 2616–2629. doi: 10.1175/JAS3771.1

Thompson, D. W. J., & Wallace, J. M. (1998, 5). The Arctic oscillation signature

in the wintertime geopotential height and temperature fields. *Geophysical Research Letters*, *25*(9), 1297–1300. doi: 10.1029/98GL00950

Vitart, F., Ardilouze, C., Bonet, A., Brookshaw, A., Chen, M., Codorean, C., ... Zhang, L. (2017). The subseasonal to seasonal (S2S) prediction project database. *Bulletin of the American Meteorological Society*, *98*(1), 163–173. doi: 10.1175/BAMS-D-16-0017.1

Weinberger, I., Garfinkel, C. I., White, I. P., & Birner, T. (2021, 6). The Efficiency of Upward Wave Propagation Near the Tropopause: importance of the form of the refractive index. *Journal of the Atmospheric Sciences*, *78*(8), 2605–2617. doi: 10.1175/JAS-D-20-0267.1

White, I., Garfinkel, C. I., Gerber, E. P., Jucker, M., Hitchcock, P., & Rao, J. (2020, 1). The generic nature of the tropospheric response to sudden stratospheric warmings. *Journal of Climate*, *33*(13), 5589–5610. doi: 10.1175/JCLI-D-19-0697.1

Supporting Information for "Ozone-forced Southern Annular Mode during Antarctic Stratospheric Warming Events"

DOI: 10.1002/2021GL095270R

M. Jucker[1], R. Goyal[1]

[1]Climate Change Research Centre and ARC Centre of Excellence for Climate Extremes, University of New South Wales, Sydney, Australia

Contents of this file

1. Figures S1 to S4

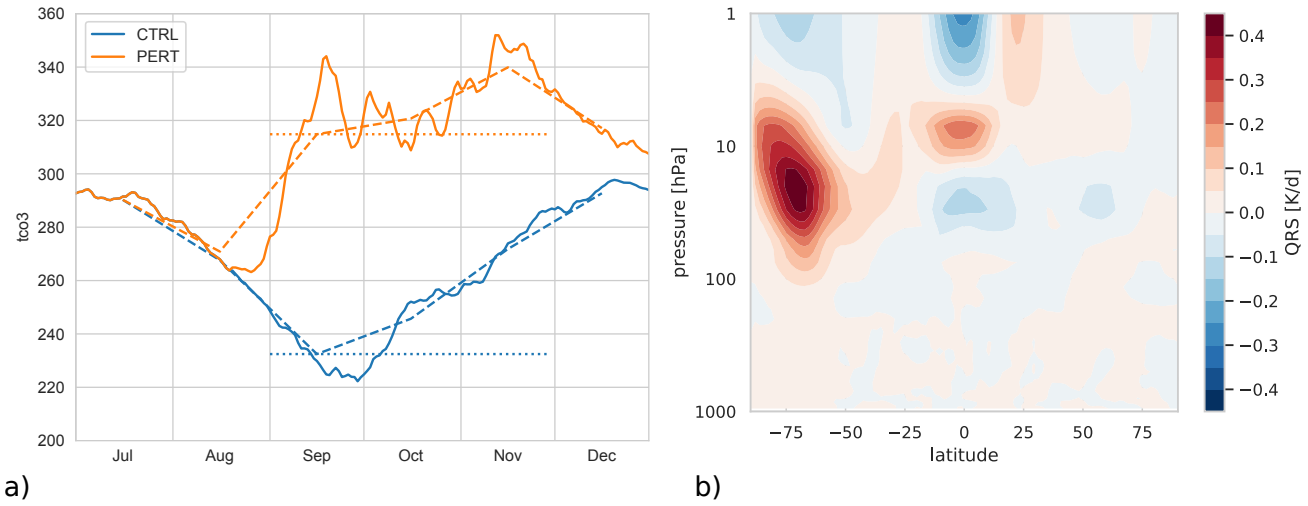

Figure S1. (a) Climatological (CTRL) and perturbation (PERT) polar cap (60-90°S) mean total column ozone. Dashed lines show linear interpolation of monthly means as used in the seasonal simulations. Dotted lines show the ozone concentrations see by the perpetual simulations. (b) Difference in time and ensemble mean shortwave heating rates between PERT-P and CTRL-P, which corresponds to the anomalous ozone heating due to 2019 September ozone.

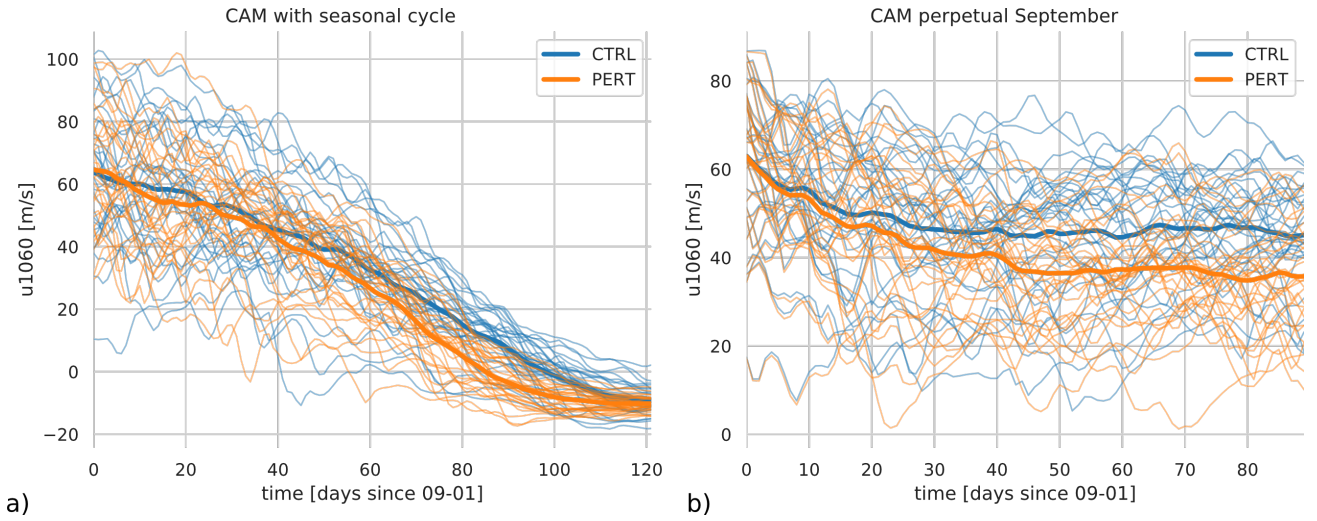

Figure S2. Zonal mean zonal wind at 60 S and 10 hPa for all members (thin lines) and ensemble mean (thick lines) in the CAM simulations with (a) seasonal cycle and (b) perpetual September setup.

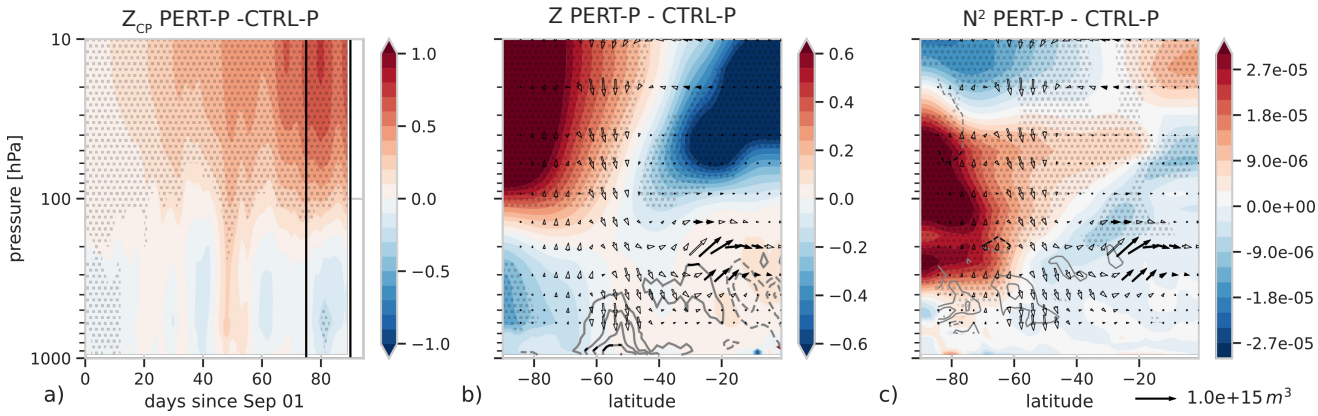

Figure S3. Same as Fig. 2 but for the perpetual simulations with CAM. Due to strong internal variability (e.g. variability across members), the tropospheric positive SAM remains weak for about 60 days, and only starts becoming statistically significant after about 80 days, when the constant ozone heating causes both the stratospheric and tropospheric anomalies to become large enough. In stark contrast to the simulations with seasonal cycle, there is no indication of a downward propagation (slow response), while the dynamical response to the ozone forcing closely resembles the fast response in the simulation with seasonal cycle.

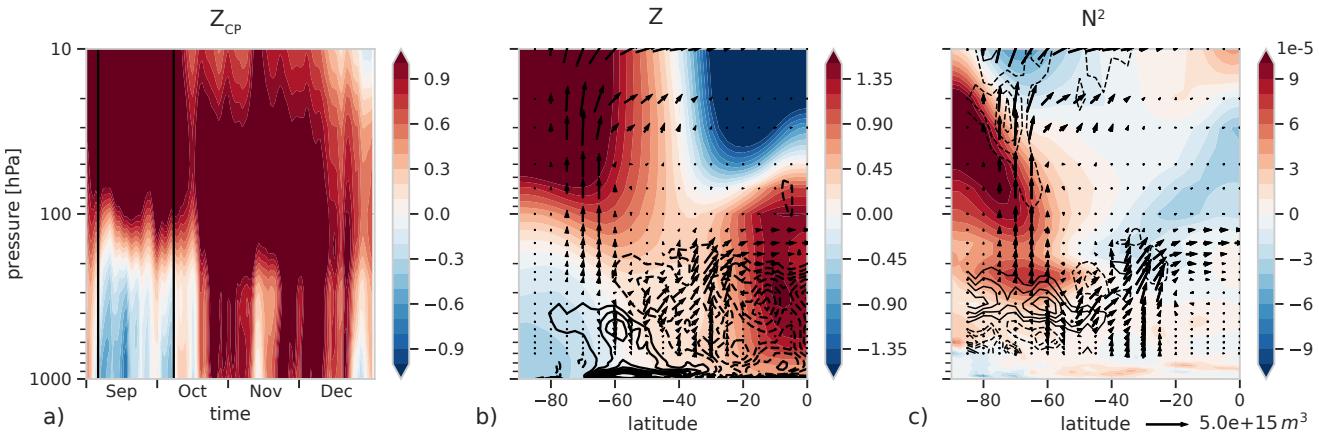

Figure S4. Same as Fig. 2 but for ERA5 data between Sep 5 and Oct 8 2019. No significance testing has been applied (single member). Even if the strong SWE occurring in 2019 increases the stratospheric perturbations and upward EP fluxes during this period compared to our model simulations without SWE, there are still many qualitative agreements between this specific observed event and our model analysis. For instance, there are anomalous equatorward EP fluxes and positive EP flux divergence just below the region of enhanced lower tropospheric stability in the extratropics (panel c), which forces an anomalous clockwise circulation centered at 60°S (panel b). Note the difference in arrow scale compared to Figs. 2 and S3. The streamfunction contours are now spaced 4e9 kg/s and EP flux divergence contours are spaced by $1\,\mathrm{ms}^{-1}\mathrm{d}^{-1}$. Anomalies are calculated relative to 1981-2010 daily climatology following the WMO climatological standard for long-term averages (`https://community.wmo.int/wmo-climatological-normals`).